Available online at www.sciencedirect.com
SCIENCE DIRECT®
Journal of Molecular Structure 660 (2003) 81–97
Journal of MOLECULAR STRUCTURE
www.elsevier.com/locate/molstruc

# Twisted amides: X-ray crystallographic and theoretical study of two acylated glycolurils with aromatic substituents

Chérif F. Matta[1], Christopher N. Cow, Paul H.M. Harrison*

*Department of Chemistry, McMaster University, 1280 Main St W., Hamilton, Ont., Canada L8S 4M1*

Received 24 June 2003; revised 6 August 2003; accepted 6 August 2003

**Abstract**

X-ray crystallography and theoretical analysis were applied to explore the molecular basis for the efficient and selective Claisen-like condensations of diacylglycolurils. The crystal structures of 1-acetyl-6-benzoyl-3,4,7,8-tetramethylglycoluril (**4b**), and of 1-(3′-oxo-3′-phenylpropionyl)-3,4,7,8-tetramethylglycoluril (**5b**), the product of base-promoted intramolecular condensation of **4b**, were obtained by X-ray diffraction. The acetyl (Ac) group in **4b** is essentially coplanar with the attached tetrahydroimidazolone ring of the glycoluril core ($\tau = 7°$), while the benzoyl (Bz) group is twisted by $\tau = 45°$ relative to a plane through the ring to which it is bonded. Product **5b** contains a flat amide ($\tau = 7°$). Ab initio energy optimizations of the experimental structures for **4b** and **5b** give optimized geometries which are not dramatically altered, suggesting that crystal packing effects are small. An atoms-in-molecules study of the delocalization of the Fermi hole reveals that electrons in the Bz C=O group of **4b** are delocalized into the phenyl ring as well as into the urea moiety of the glycoluril core. This effect stabilizes the Bz over the Ac carbonyl group, and accounts for selective twisting of the Bz group. The Laplacian of the electron density reveals a non-bonded valence shell charge concentration at O of the Ac group, corresponding to a lone-pair region, aligned with a charge depletion in the valence shell of the Bz C=O carbon [$\angle$(C15–O16···C18) = 113°]. The angle of approach [$\angle$(O16···C18=O19)] is 100°, equal to the angle for ideal nucleophilic attack on a carbonyl group. Oxygen atom O16 is thus poised to attack C18; only the O16···C18 distance (3.248 Å) seems to prevent reaction. These results suggest that the same distance restraint may prevent O-acylation in the enolate intermediate **6b** derived from **4b**. By contrast, the transition state for C-acylation, leading from **6b** towards product **5b** requires a different geometry, which may explain the observed selectivity for C-acylation in this enolate. The results show that, as **4b** is converted to **5b**, amide torsional strain is relieved, which may account for the high reactivity of **4b** and the efficiency and irreversibility of this condensation process. This study provides a starting point for quantitative correlation of substrate structure in diacylglycolurils with kinetic data for the rearrangement reaction.


*Keywords:* Glycoluril; Claisen condensation; X-ray diffraction; Crystal structure; Twisted amide; Atoms-in-molecules

## 1. Introduction

The fatty acids and polyketides are a diverse group of natural products that derive from 'head-to-tail' Claisen-like condensations of acyl precursors [1,2]. In a novel approach to synthesis of this class of

* Corresponding author. Tel.: +1-905-525-9140; (ext.27290); Fax: 1-905-522-2509.
*E-mail address:* pharriso@mcmaster.ca (P.H.M. Harrison).
[1] Present address: Lash Miller Chemical Laboratories, Department of Chemistry, University of Toronto, Toronto, Ont., Canada M5S 3H6.

0022-2860/$ - see front matter © 2003 Elsevier B.V. All rights reserved.
doi:10.1016/j.molstruc.2003.08.005

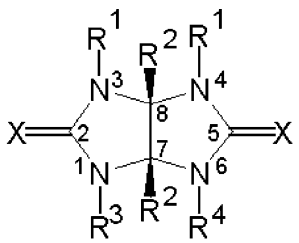

| Compound | $R^1$ | $R^2$ | $R^3$ | $R^4$ | X |
|---|---|---|---|---|---|
| **1** | Me | Me | H | H | O |
| **2** | Me | Me | H | H | S |
| **3** | Me | Me | Ac | H | O |
| **4a** | Me | Me | Ac | Ac | O |
| **4b** | Me | Me | Ac | Bz | O |
| **4c** | Me | Me | Ac | Ac | S |
| **4d** | Me | Me | $Me_3CCO$ | $Me_3CCO$ | S |
| **5a** | Me | Me | $MeCOCH_2CO$ | H | O |
| **5b** | Me | Me | $PhCOCH_2CO$ | H | O |
| **8** | H | H | H | H | O |
| **9** | H | Me | H | H | O |
| **10** | H | $NH_2$ | H | H | O |
| **11** | Me | H | H | H | O |

Fig. 1. Structure of glycoluril derivatives referred to in the text.

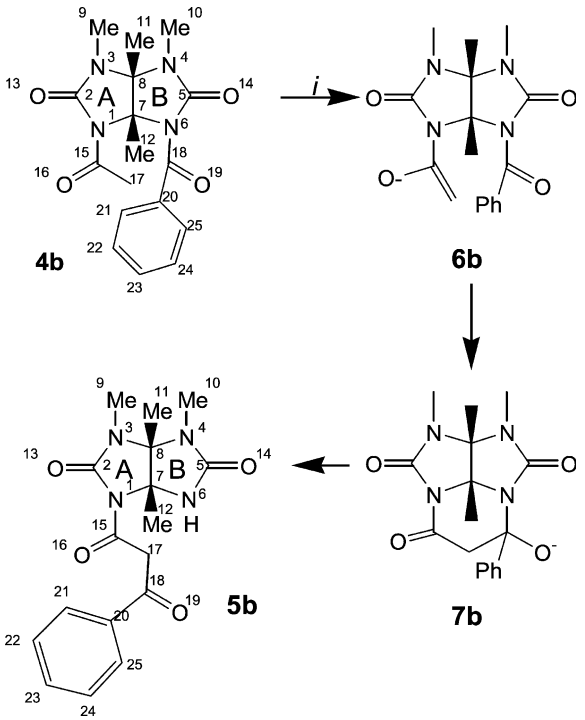


Scheme 1. The numbering system for **4b** and **5b** and the definition of rings **A** and **B** are shown. Reagents: (i) KOtBu, THF, 0 °C, 20 min.

compounds, we used glycolurils **1** [3] or **2** [4] (Fig. 1) as biomimetic templates to hold and orient two acyl groups for base-promoted condensation. Thus two sequential or concomitant acylations with acyl halides or anhydrides at the N1 and N6 positions of **1** or **2** give a variety of mono- (e.g. **3**) and di-acylglycolurils (e.g. **4a**–**d**). Efficient intramolecular condensations in **4** then furnish β-ketoacylglycolurils **5** (e.g. **4a** gives **5a**), in a reaction reminiscent of the Claisen condensation [3–7]. A variety of further transformations of **5** through iterative sequences that resemble the assembly of fatty acids and polyketides subsequently allows for preparation of oligoketides [5–7].

These prior studies focused on aliphatic acyl groups. Recently, we reported the extension of this methodology to aroyl groups as the electrophilic acyl donors in the key C–C bond formation step, including the highly efficient conversion of **4b** to **5b** (Scheme 1) [8]. We also undertook a detailed investigation of the mechanism of this reaction through kinetics experiments that enabled quantitative rate data to be obtained for the condensation reaction. The results were consistent with a process in which **4b** was deprotonated to give enolate **6b**, which then proceeded through the key C–C bond-forming step to tetrahedral intermediate **7b**. Collapse of **7b** rapidly gives product **5b** after work up. Both of the first two steps, the generation of **6b** and its conversion to **7b**, control the overall rate of formation of **5b**, as shown by isotope effects and the influence of substituents in the aromatic ring.

During this work, we sought to better understand the structural and geometric factors that lead to the high rate of the condensation reaction; that give rise to the established specificity for C-acylation over O-acylation in the intermediate enolate (e.g. **6b**); and that regulate the thermodynamic effects that lead to complete conversion of **4** to **5**. Thus, we examined the X-ray crystallographic geometries of a variety of these glycoluril derivatives, including **1** [9] and **3** [10], as well as diacylglycolurils **4a** [10], **4c** [11], and **4d** [12]. While **1** possesses a crystallographic plane of symmetry, as was found for unsubstituted glycoluril (**8**) [13,14] as well as

7,8-dimethyl glycoluril (**9**) [15], all the acylated glycolurils examined were asymmetric, with the two bridgehead-to-bridgehead substituent bonds twisting out of the eclipsed geometry ($\angle R^2 - C7-C8-R^2 \neq 0$, Fig. 1). Similar twists have been reported for other symmetrically-substituted structures such as **10** [16] and **11** [17], as well as for 1,4-dinitroglycoluril [18,19].

Another interesting aspect of the crystal structures of diacylglycolurils **4a**, **c** and **d** was the observed acyl group geometries: one (in **4a** and **4c**) or both (in **4d**) acyl groups are twisted around the N–C bond, such that the acyl Cα–C=O and the C2–N1–C7 or C5–N6–C7 planes of the attached rings are non-parallel. For example, **4a** has one acetyl group which is essentially coplanar with the attached 5-membered ring ($\tau_A = -0.3°$), where $\tau$ is the amidic twist angle, as defined by Dunitz [20] and modified by Yamada [21] (e.g. $\tau_A = 180 - [(\angle C7-N1-C15-C17) + (\angle C2-N1-C15-O16)]/2$, see Scheme 1) [10]. However, the second acetyl group is twisted ($\tau_B = 17.2°$), where **A** and **B** refer to the two sides of the molecule, see Scheme 1 [10]. Compounds **4c** and **4d** exhibit more dramatic twists. These molecules therefore are examples of twisted amides, an important class of compounds that has been proposed to mimic the transition state in protease-catalysed amide hydrolysis as well as *cis/trans* peptide isomerases [22]. Twisted amides also exhibit a variety of non-amidic spectral characteristics [22], and chemical properties such as high reactivity towards nucleophiles at the carbonyl carbon [22]. We therefore reasoned that twisting might be intimately involved in the reactivity of these diacylglycolurils in the Claisen-like condensation. The crystal geometries of twisted amides often exhibit long N–C(=O) bonds. Indeed, lengthening of the C–N bond was observed in the twisted acyl groups of **4a**, **4c** and **4d**, relative to the untwisted acyl moieties, and **4d** had one of the longest N–C bonds known in such compounds.

Each of the molecules we studied had two identical aliphatic acyl groups, and can in principle adopt a variety of symmetric conformations, but choose to adopt asymmetric ones. Since the experimental geometries of **3** and **4a** were reproduced by full ab initio geometry optimizations of the isolated molecules, we suggested that crystal packing effects are not the major cause of their asymmetric geometry [10]. Rather, we proposed that the close proximity of two negatively charged acyl carbonyl oxygen atoms prohibits the simultaneous planarity of both amidic linkages. One amide endeavours to remain planar, maintaining stability, while the other twists to relieve an unfavourable closed-shell O–O interaction. The twisting of the glycoluril core itself was then explained by the resulting asymmetry in the extent to which electron density at N1 and N6 could delocalize into the attached acyl carbonyl groups. This effect leads to different electron densitites at these two nitrogen atoms, and hence to an anomeric-like effect at aminal carbon C7, leading to the twisting of the bridgehead (C11–C8–C7–C12) dihedral angle [10].

These molecules can in principle still adopt a conformation in which both acyl groups are equally twisted, thereby keeping the acyl carbonyl oxygen atoms apart while the core remains symmetric, but fail to do so. We have continued to explore these structures to further understand their geometry. Herein we present a rationale for the observed geometry of these compounds, deduced from an examination of **4b**, in which an inherent asymmetry is present due to the two different acyl entities. The experimental crystallographic and ab initio theoretical geometries for both **4b** and **5b** are compared, and also correlated with our previously reported calculations [10] for **4a** and **3**, respectively. The results support and extend our hypothesis for the origin of both acyl group and bridgehead twisting in diacylglycolurils [10–12]. Then an atoms-in-molecules (AIM) study was undertaken to reveal a favorable interaction that stabilizes the twisted, asymmetric structure. Finally, the results are discussed in terms of the geometric requirements for the reaction of **4b** to give **5b**, and the structures are used to generate a hypothesis for explanation of the efficiency and selectivity of the condensation reaction.

## 2. Methods and results

### 2.1. X-ray crystallographic study

Microscopic examination of crystals of **4b** grown by slow diffusion of hexanes into $CHCl_3$ revealed two crystal habits: a dominant sheet-like form, which was selected for the X-ray experiment, and a minor needle-prismatic form. Compound **5b** was

Table 1
Crystal and refinement data for compounds **4b** and **5b**

| | **4b** | **5b** |
|---|---|---|
| Empirical formula | $C_{17}H_{20}N_4O_4{\cdot}CHCl_3$ | $C_{17}H_{20}N_4O_4$ |
| Formula weight | 463.74 | 344.37 |
| Temperature | 300(2) K | 300(2) K |
| Wavelength | 0.71073 Å | 0.71073 Å |
| Crystal system | Monoclinic | Monoclinic |
| Space group | *P*2(1)/*n* | *C*2/*c* |
| $a, \alpha$ | 9.456(6) Å, 90° | 24.1547(9) Å, 90° |
| $b, \beta$ | 20.874(14) Å, 106.99(3)° | 10.9783(4) Å, 112.9960(10)° |
| $c, \gamma$ | 11.641(7) Å, 90° | 13.7526(5) Å, 90° |
| Volume, *Z* | 2198(2) $Å^3$, 4 | 3357.1(2) $Å^3$, 8 |
| Density (calculated) | 1.402 $mg/m^3$ | 1.363 $mg/m^3$ |
| Absorption coefficient | 0.448 $mm^{-1}$ | 0.099 $mm^{-1}$ |
| *F*(000) | 960 | 1456 |
| Crystal size | $0.03 \times 0.18 \times 0.48$ $mm^3$ | $0.10 \times 0.14 \times 0.27$ $mm^3$ |
| $\theta$ Range for data collection | 1.95–26.43° | 2.07–25.00° |
| Limiting indices | $-11 \le h \le 11, -26 \le k \le 26, -13 \le l \le 13$ | $-30 \le h \le 27, 0 \le k \le 13, 0 \le l \le 17$ |
| Reflections collected | 13,783 | 2880 |
| Independent reflections | 4325 [$R_{int} = 0.0595$] | 2880 |
| Refinement method | Full-matrix-least-squares on $F^2$ | Full-matrix-least-squares on $F^2$ |
| Data/restraints/parameters | 4325/0/263 | 2814/0/307 |
| Goodness-of-fit on $F^2$ | 1.061 | 1.143 |
| Final *R* indices [$I > 2\sigma(I)$] | $R1 = 0.0828, wR2 = 0.1943$ | $R1 = 0.0718, wR2 = 0.1453$ |
| *R* indices (all data) | $R1 = 0.1581, wR2 = 0.2441$ | $R1 = 0.1227, wR2 = 0.1796$ |
| Extinction coefficient | 0.0026(14) | 0.0023(5) |
| Largest diff. peak and hole | 0.400 and $-0.377e$ $Å^{-3}$ | 0.221 and $-0.227e$ $Å^{-3}$ |

crystallized by slow evaporation from $CHCl_3$ and the crystals exhibited a single needle-prismatic crystal habit. A single crystal of each compound was mounted on a RIGAKU AFC6/RA diffractometer. Diffraction patterns were obtained and solved by direct methods as implemented in the Siemens SHELXTL program. Table 1 gives crystal data and structure refinement details for the two compounds.

Final atomic co-ordinates and equivalent isotropic thermal parameters are given in Table 2. Anisotropic displacement parameters are listed in Table 3. Bond lengths, angles and selected dihedral angles are listed in Tables 4–6. Table 7 lists the experimental ring conformations and puckering parameters, as well as the calculated values (see below). The conformational descriptors are as previously defined [10], and include the bridgehead dihedral angle ∠C11–C8–C7–C12 ($\eta$); the angle ($\Xi$) between the mean (least square [23]) planes of the two 5-membered rings **A** and **B**; the ring coordinates in conformational space ($Q$ and $\phi$) as described by Cremer and Pople [24] which were obtained using the RING program [25]; and the amide twist angles ($\tau$) as defined by Yamada (see above). Fig. 2 shows the crystal packing of **4b** and **5b**, while thermal ellipsoid drawings of both molecules, along with the numbering scheme, are presented in Fig. 3.

### 2.2. Computational methods

The X-ray geometries of compounds **4b** and **5b** were each subjected to full geometry optimizations at the restricted Hartree–Fock (RHF)/3-21G level. The bridgehead dihedral angles Me–C–C–Me ($\eta$) along with $\Xi$, $\tau$, $Q$, $\phi$ and a brief description of the ring conformations were obtained from the optimized geometries as described above for the experimental ones and are presented in Table 7. The optimized geometries of both **4b** and **5b** generally reproduce the corresponding experimental ones to a reasonable degree. A set of comparison statistics is displayed in

Table 2
Atomic coordinates ( $\times 10^4$) and equivalent isotropic displacement parameters ( $\times 10^3$ Å$^2$) for **4b** (and $CHCl_3$ solvent molecule) and **5b**

| Atom | **4b** | | | | **5b** | | | |
|---|---|---|---|---|---|---|---|---|
| | *x* | *y* | *z* | $U_{eq}$ | *x* | *y* | *z* | $U_{eq}$ |
| N1 | 6541(4) | −1971(2) | 8787(3) | 44(1) | 3773(1) | 375(3) | 624(2) | 34(1) |
| C2 | 6758(5) | −1908(2) | 7651(4) | 50(1) | 3242(2) | 865(4) | −130(3) | 41(1) |
| N3 | 8072(4) | −2172(2) | 7704(3) | 52(1) | 2788(1) | 502(3) | 137(2) | 46(1) |
| N4 | 9958(4) | −1955(2) | 9563(3) | 47(1) | 3084(1) | 719(3) | 2028(2) | 45(1) |
| C5 | 9800(5) | −1806(2) | 10,651(4) | 42(1) | 3654(2) | 597(3) | 2797(3) | 43(1) |
| N6 | 8448(4) | −2062(2) | 10,694(3) | 39(1) | 3967(2) | −192(3) | 2433(2) | 41(1) |
| C7 | 7682(4) | −2396(2) | 9579(4) | 39(1) | 3642(2) | −482(3) | 1337(3) | 37(1) |
| C8 | 8877(5) | −2409(2) | 8885(4) | 42(1) | 2989(2) | −115(3) | 1152(3) | 39(1) |
| C9 | 8587(7) | −2224(4) | 6646(5) | 90(2) | 2169(2) | 877(7) | −479(4) | 67(2) |
| C10 | 11,261(5) | −1750(3) | 9224(5) | 58(1) | 2614(3) | 1194(7) | 2316(5) | 75(2) |
| C11 | 9575(6) | −3058(3) | 8807(5) | 62(1) | 2572(2) | −1137(5) | 1156(5) | 63(1) |
| C12 | 7024(6) | −3038(2) | 9744(5) | 57(1) | 3735(2) | −1769(4) | 1063(4) | 51(1) |
| O13 | 5890(4) | −1678(2) | 6776(3) | 72(1) | 3204(1) | 1488(3) | −878(2) | 52(1) |
| O14 | 10,665(3) | −1521(2) | 11,452(3) | 53(1) | 3843(1) | 1092(3) | 3654(2) | 60(1) |
| C15 | 5399(5) | −1698(2) | 9171(5) | 52(1) | 4354(2) | 556(3) | 692(3) | 38(1) |
| O16 | 5269(4) | −1846(2) | 10,128(4) | 70(1) | 4753(1) | −58(3) | 1322(2) | 54(1) |
| C17 | 4412(6) | −1219(3) | 8373(5) | 66(2) | 4463(2) | 1519(4) | 19(3) | 44(1) |
| C18 | 7996(5) | −2034(2) | 11,758(4) | 45(1) | 4306(2) | 2777(4) | 247(3) | 43(1) |
| O19 | 7516(4) | −2498(2) | 12,125(3) | 61(1) | 4210(2) | 2978(3) | 1036(2) | 63(1) |
| C20 | 8132(5) | −1403(2) | 12,365(4) | 46(1) | 4274(2) | 3786(4) | −495(3) | 43(1) |
| C21 | 8018(6) | −828(3) | 11,750(5) | 62(1) | 4168(2) | 4955(4) | −242(4) | 53(1) |
| C22 | 8076(8) | −255(3) | 12,361(7) | 87(2) | 4138(2) | 5917(5) | −896(4) | 67(1) |
| C23 | 8256(9) | −259(4) | 13,577(8) | 100(2) | 4212(3) | 5721(6) | −1817(4) | 77(2) |
| C24 | 8357(8) | −822(4) | 14,178(6) | 95(2) | 4318(3) | 4570(6) | −2088(4) | 85(2) |
| C25 | 8296(6) | −1396(3) | 13,587(5) | 60(1) | 4351(2) | 3595(5) | −1426(3) | 69(1) |
| CHCl3 | | | | | | | | |
| C26 | 7580(8) | 260(3) | 7860(6) | 87(2) | | | | |
| Cl27 | 6236(3) | 481(1) | 8515(2) | 129(1) | | | | |
| Cl28 | 8517(3) | −428(1) | 8539(3) | 138(1) | | | | |
| Cl29 | 6807(4) | 127(1) | 6352(2) | 167(1) | | | | |

$U_{eq}$ is defined as one-third of the trace of the orthogonalized $U_{ij}$ tensor.

Table 8, to provide quantitative measures of agreement between the observed and calculated geometries.

The optimized geometries were then used in single point calculations to obtain wavefunctions at the RHF/6-311G** level using the GAUSSIAN94 package [26]. These wavefunctions were then analyzed within the framework of the AIM theory. The electron density of **4b** was analyzed using AIMPAC [27], and the delocalization indices were computed using AIMDELOC [28]. Fig. 4(a) displays the resulting optimized geometry of **4b**, labeled with key calculated bond lengths. The delocalization indices between bonded atoms in the moiety of interest along with the electron densities at the bond critical points are given in Fig. 4(b). Fig. 4(c) shows the integrated atomic charges on selected atoms in **4b**. Fig. 5 shows a three-dimensional plot of the zero-Laplacian envelope of **4b** ($\nabla^2\rho(\mathbf{r})$).

## 3. Discussion

### 3.1. Experimental molecular geometry of *4b*

The geometry of **4b** resembles that of diacetylglycoluril (**4a**) in many respects. When the two structures

Table 3
Anisotropic displacement parameters ( $\times 10^3$ Å$^2$) for **4b** and **5b**

| | **4b** | | | | | | **5b** | | | | | |
|---|---|---|---|---|---|---|---|---|---|---|---|---|
| | $U_{11}$ | $U_{22}$ | $U_{33}$ | $U_{23}$ | $U_{13}$ | $U_{12}$ | $U_{11}$ | $U_{22}$ | $U_{33}$ | $U_{23}$ | $U_{13}$ | $U_{12}$ |
| N1 | 35(2) | 56(2) | 41(2) | 0(2) | 13(2) | −1(2) | 30(2) | 42(2) | 28(2) | 6(1) | 9(1) | 5(1) |
| C2 | 47(3) | 65(3) | 36(3) | −1(2) | 11(2) | −7(2) | 37(2) | 50(2) | 29(2) | 5(2) | 5(2) | 8(2) |
| N3 | 46(2) | 76(3) | 38(2) | −1(2) | 20(2) | 3(2) | 32(2) | 69(2) | 33(2) | 8(2) | 6(1) | 8(2) |
| N4 | 38(2) | 64(3) | 45(2) | −1(2) | 23(2) | −12(2) | 47(2) | 52(2) | 39(2) | −1(2) | 18(2) | 14(2) |
| C5 | 41(2) | 48(3) | 42(3) | −2(2) | 17(2) | 0(2) | 52(2) | 40(2) | 36(2) | 4(2) | 15(2) | −2(2) |
| N6 | 35(2) | 50(2) | 36(2) | −2(2) | 17(2) | −6(2) | 34(2) | 56(2) | 27(2) | −2(1) | 7(1) | 0(2) |
| C7 | 36(2) | 48(3) | 37(2) | −4(2) | 15(2) | −4(2) | 35(2) | 42(2) | 31(2) | −1(2) | 1(2) | 1(2) |
| C8 | 35(2) | 55(3) | 39(3) | −9(2) | 14(2) | −7(2) | 38(2) | 43(2) | 35(2) | 0(2) | 14(2) | 0(2) |
| C9 | 72(4) | 164(7) | 41(3) | −3(4) | 27(3) | −2(4) | 33(2) | 107(5) | 50(3) | 16(3) | 5(2) | 15(3) |
| C10 | 41(3) | 81(4) | 61(3) | −1(3) | 29(2) | −14(2) | 73(4) | 91(5) | 64(3) | 11(3) | 31(3) | 39(4) |
| C11 | 58(3) | 67(3) | 66(4) | −21(3) | 25(3) | 5(3) | 51(3) | 64(3) | 74(4) | 2(3) | 24(3) | −13(3) |
| C12 | 57(3) | 57(3) | 57(3) | −9(3) | 19(3) | −14(2) | 60(3) | 38(2) | 52(3) | 0(2) | 19(2) | 5(2) |
| O13 | 58(2) | 107(3) | 45(2) | 8(2) | 8(2) | 1(2) | 44(2) | 69(2) | 38(2) | 18(1) | 9(1) | 12(1) |
| O14 | 46(2) | 71(2) | 45(2) | −19(2) | 16(2) | −14(2) | 82(2) | 56(2) | 35(2) | −1(1) | 17(1) | −6(2) |
| C15 | 36(3) | 61(3) | 61(3) | −4(3) | 18(2) | −6(2) | 35(2) | 49(2) | 30(2) | −3(2) | 13(2) | 2(2) |
| O16 | 53(2) | 104(3) | 65(3) | 9(2) | 36(2) | 12(2) | 34(1) | 78(2) | 40(2) | 12(2) | 6(1) | 13(1) |
| C17 | 49(3) | 65(3) | 84(4) | 7(3) | 23(3) | 7(3) | 36(2) | 60(3) | 42(2) | −4(2) | 20(2) | −1(2) |
| C18 | 41(2) | 61(3) | 39(3) | 4(2) | 20(2) | 3(2) | 37(2) | 61(3) | 26(2) | −5(2) | 8(2) | −4(2) |
| O19 | 74(2) | 65(2) | 55(2) | 9(2) | 37(2) | −4(2) | 90(2) | 62(2) | 45(2) | −4(1) | 37(2) | −4(2) |
| C20 | 41(2) | 64(3) | 38(3) | −7(2) | 17(2) | 4(2) | 33(2) | 59(3) | 33(2) | −3(2) | 9(2) | −7(2) |
| C21 | 64(3) | 63(4) | 64(3) | 3(3) | 26(3) | 15(3) | 47(2) | 63(3) | 49(3) | 1(2) | 20(2) | −5(2) |
| C22 | 90(5) | 61(4) | 114(6) | −12(4) | 36(4) | 13(3) | 60(3) | 66(4) | 70(3) | 8(3) | 20(2) | −4(3) |
| C23 | 109(6) | 89(6) | 110(6) | −46(5) | 44(5) | −2(4) | 80(4) | 80(4) | 58(3) | 19(3) | 15(3) | −18(3) |
| C24 | 109(6) | 121(7) | 58(4) | −29(5) | 29(4) | −1(5) | 114(5) | 101(5) | 38(3) | 8(3) | 29(3) | −15(4) |
| C25 | 61(3) | 75(4) | 49(3) | −8(3) | 23(2) | −1(3) | 87(4) | 76(4) | 44(3) | −4(2) | 27(2) | −13(3) |
| Solv. | | | | | | | | | | | | |
| C26 | 111(5) | 55(4) | 104(5) | −15(4) | 46(4) | −23(3) | | | | | | |
| Cl27 | 142(2) | 112(2) | 161(2) | −32(2) | 88(2) | −27(1) | | | | | | |
| Cl28 | 117(2) | 118(2) | 173(2) | 42(2) | 33(2) | 1(1) | | | | | | |
| Cl29 | 256(4) | 142(2) | 97(2) | −22(2) | 41(2) | 23(2) | | | | | | |

The anisotropic displacement factor exponent takes the form: $-2\pi^2[h^2(a^*)^2U_{11} + \cdots + 2\,hka^*b^*U_{12}]$.

are overlaid (Fig. 6a), it is apparent that there are small differences in the ring system and acyl groups. The differences may be summarized by considering the set of ring conformation descriptors defined earlier: $\eta, \Xi$, describing the relative orientation of the two rings; and the Cramer–Pople parameters $Q$ and $\phi$ describing the conformation of each of the 5-membered rings of the glycoluril core (Table 7 and Table 9 of ref.[10]). The rings in **4b** are slightly more pushed apart from each other (larger $\Xi$) and somewhat flatter (smaller puckering amplitude $Q$) than in **4a** and adopt different conformations. These effects at first sight appear to be the result of the larger benzoyl group the phenyl group of which is located on the endo side of the bicyclic entity, where steric interactions between the atoms of the phenyl group and ring **A** are relieved as $\Xi$ increases. These interactions may lead to the small reduction in $\eta$ in **4b** compared to **4a**: as $\Xi$ increases, it becomes more difficult to push C11 to one side.

In **4a**, one acetyl group is twisted around the N–C(=O) bond while the other is flat, raising the question of which acyl group would twist in an asymmetrically substituted glycoluril. The crystal structure of **4b** shows that it is

Table 4
Bond lengths (Å) for **4b** and **5b**

| | 4b | 5b |
|---|---|---|
| N1–C2 | 1.403(6) | 1.403(4) |
| N1–C7 | 1.490(6) | 1.480(4) |
| N1–C15 | 1.404(6) | 1.384(5) |
| C2–N3 | 1.344(6) | 1.347(5) |
| C2–O13 | 1.205(6) | 1.209(4) |
| N3–C8 | 1.450(6) | 1.453(4) |
| N3–C9 | 1.455(6) | 1.460(5) |
| N4–C5 | 1.355(6) | 1.377(5) |
| N4–C8 | 1.447(5) | 1.457(5) |
| N4–C10 | 1.463(5) | 1.439(6) |
| C5–N6 | 1.400(5) | 1.366(5) |
| C5–O14 | 1.202(5) | 1.214(4) |
| N6–C7 | 1.465(5) | 1.437(4) |
| N6–C18 | 1.425(5) | |
| C17–C18 | | 1.497(6) |
| C7–C8 | 1.570(6) | 1.550(5) |
| C7–C12 | 1.513(6) | 1.502(5) |
| C8–C11 | 1.521(7) | 1.508(6) |
| C15–O16 | 1.196(6) | 1.217(4) |
| C15–C17 | 1.493(7) | 1.495(5) |
| C18–O19 | 1.201(5) | 1.215(4) |
| C18–C20 | 1.483(7) | 1.488(5) |
| C20–C21 | 1.386(7) | 1.378(6) |
| C20–C25 | 1.384(7) | 1.381(6) |
| C21–C22 | 1.383(8) | 1.370(7) |
| C22–C23 | 1.375(10) | 1.364(7) |
| C23–C24 | 1.357(10) | 1.370(8) |
| C24–C25 | 1.375(9) | 1.387(7) |

Table 5
Bond angles (°) for **4b** and **5b**

| | 4b | 5b |
|---|---|---|
| N1–C2–N3 | 107.8(4) | 106.9(3) |
| N1–C2–O13 | 125.7(5) | 126.2(4) |
| N1–C7–N6 | 110.2(3) | 112.6(3) |
| N1–C7–C8 | 101.1(3) | 101.2(3) |
| N1–C7–C12 | 110.8(4) | 109.9(3) |
| N1–C15–O16 | 119.3(5) | 117.9(3) |
| N1–C15–C17 | 118.2(5) | 118.6(3) |
| C2–N1–C7 | 111.1(4) | 111.3(3) |
| C2–N1–C15 | 126.9(4) | 127.2(3) |
| C2–N3–C8 | 114.0(4) | 113.5(3) |
| C2–N3–C9 | 121.6(4) | 121.1(4) |
| N3–C2–O13 | 126.5(5) | 126.9(3) |
| N3–C8–N4 | 112.6(4) | 112.7(3) |
| N3–C8–C7 | 102.9(3) | 102.4(3) |
| N3–C8–C11 | 111.3(4) | 112.2(4) |
| N4–C5–N6 | 107.3(4) | 108.1(3) |
| N4–C5–O14 | 127.1(4) | 125.9(4) |
| N4–C8–C7 | 102.0(3) | 101.8(3) |
| N4–C8–C11 | 111.5(4) | 110.8(4) |
| C5–N4–C8 | 114.0(3) | 111.2(3) |
| C5–N4–C10 | 121.1(4) | 118.9(4) |
| C5–N6–C7 | 111.8(3) | 111.7(3) |
| C5–N6–C18 | 121.6(4) | |
| N6–C5–O14 | 125.6(4) | 126.0(4) |
| N6–C7–C8 | 102.7(3) | 102.7(3) |
| N6–C7–C12 | 115.1(4) | 113.4(3) |
| N6–C18–O19 | 121.1(4) | |
| C17–C18–O19 | | 120.5(4) |
| N6–C18–C20 | 116.4(4) | |
| C17–C18–C20 | | 119.5(3) |
| C7–N1–C15 | 122.0(4) | 121.4(3) |
| C7–N6–C18 | 126.4(3) | |
| C7–C8–C11 | 115.9(4) | 116.3(4) |
| C8–N3–C9 | 124.4(4) | 124.8(4) |
| C8–N4–C10 | 124.1(4) | 124.6(4) |
| C8–C7–C12 | 115.7(4) | 116.5(3) |
| C15–C17–C18 | | 113.7(3) |
| O16–C15–C17 | 122.5(5) | 123.5(4) |
| C18–C20–C21 | 122.7(4) | 119.0(3) |
| C18–C20–C25 | 117.8(5) | 122.2(4) |
| O19–C18–C20 | 122.5(4) | 120.0(4) |
| C20–C21–C22 | 119.8(6) | 121.3(4) |
| C20–C25–C24 | 119.9(6) | 119.8(5) |
| C21–C20–C25 | 119.4(5) | 118.7(4) |
| C21–C22–C23 | 119.9(7) | 119.7(6) |
| C22–C23–C24 | 120.3(7) | 120.2(5) |
| C23–C24–C25 | 120.7(6) | 120.2(5) |

the benzoyl group which twists significantly ($\tau = +44.8°$), while the acetyl group remains essentially coplanar with the ring ($\tau = -7.2°$). The benzoyl unit twist in **4b** is significantly more pronounced than the twist of the second acetyl group in **4a** (+17.2°) [10]. This twist is the largest in the diacylglycolurils studied to date (although smaller than in thio analogues) [11,12].

Benzoyl is the largest acyl group in a tetramethylglycoluril yet investigated crystallographically to our knowledge, and it is thus tempting to suggest that steric factors are important in influencing which of the amide groups twists. The benzoyl group can avoid a closed-shell close contact of both the phenyl ring and with carbonyl oxygen O14 by twisting in this manner. Indeed, using a molecular modeling program [29] to modify the X-ray geometry of **4b** so that the dihedral angle ∠C5–N6–C18–C20 is −20° (without changing any other geometrical parameter), results in a H21 to O14 separation of only 0.96 Å (the hydrogen atoms were added at

Table 6
Selected dihedral angles (°) for **4b** and **5b**

| | 4b | 5b |
|---|---|---|
| N1–C2–N3–C8 | −2.5(5) | −7.5(4) |
| N1–C2–N3–C9 | 175.8(5) | −178.8(4) |
| N1–C7–C8–N3 | −16.4(4) | −20.6(3) |
| N1–C7–C8–N4 | 100.5(4) | 96.2(3) |
| N1–C7–C8–C11 | −138.1(4) | −143.3(4) |
| N1–C15–C17–C18 | | −61.8(5) |
| C2–N1–C7–N6 | 124.5(4) | 127.1(3) |
| C2–N1–C7–C8 | 16.4(4) | 18.1(4) |
| C2–N1–C7–C12 | −106.9(4) | −105.6(4) |
| C2–N1–C15–O16 | 172.6(5) | 171.3(3) |
| C2–N1–C15–C17 | −9.0(7) | −10.8(5) |
| C2–N3–C8–N4 | −96.6(5) | −90.2(4) |
| C2–N3–C8–C7 | 12.5(5) | 18.4(4) |
| C2–N3–C8–C11 | 137.3(4) | 143.9(4) |
| N4–C5–N6–C7 | 0.1(5) | −8.8(4) |
| N4–C5–N6–C18 | 174.9(4) | |
| C5–N4–C8–N3 | 124.8(4) | 125.7(3) |
| C5–N4–C8–C7 | 15.1(5) | 16.7(4) |
| C5–N4–C8–C11 | −109.2(4) | −107.7(4) |
| C5–N6–C7–N1 | −98.3(4) | −89.4(4) |
| C5–N6–C7–C8 | 8.7(4) | 18.6(4) |
| C5–N6–C7–C12 | 135.4(4) | 145.1(4) |
| C5–N6–C18–O19 | −132.7(5) | |
| C5–N6–C18–C20 | 48.2(6) | |
| N6–C7–C8–N3 | −130.3(4) | −137.0(3) |
| N6–C7–C8–N4 | −13.4(4) | −20.3(4) |
| N6–C7–C8–C11 | 108.0(4) | 100.2(4) |
| N6–C18–C20–C21 | 29.5(6) | |
| N6–C18–C20–C25 | −154.3(4) | |
| C7–N1–C2–N3 | −9.6(5) | −7.8(4) |
| C7–N1–C2–O13 | 168.0(5) | 171.9(4) |
| C7–N1–C15–O16 | −5.5(7) | −3.7(5) |
| C7–N1–C15–C17 | 173.0(4) | 174.2(3) |
| C7–N6–C18–O19 | 41.4(7) | |
| C7–N6–C18–C20 | −137.7(4) | |
| C8–N4–C5–N6 | −10.2(5) | −6.0(4) |
| C8–N4–C5–O14 | 168.0(5) | 173.1(4) |
| C9–N3–C8–N4 | 85.1(6) | 80.8(5) |
| C9–N3–C8–C7 | −165.8(5) | −170.6(4) |
| C9–N3–C8–C11 | −41.0(7) | −45.1(6) |
| C10–N4–C5–N6 | 179.5(4) | −161.6(5) |
| C10–N4–C5–O14 | −2.3(8) | 17.6(7) |
| C10–N4–C8–N3 | −65.2(6) | −80.4(5) |
| C10–N4–C8–C7 | −174.9(4) | 170.6(4) |
| C10–N4–C8–C11 | 60.8(6) | 46.3(6) |
| C12–C7–C8–N3 | 103.4(4) | 98.5(4) |
| C12–C7–C8–N4 | −139.7(4) | −144.8(3) |
| C12–C7–C8–C11 | −18.3(6) | −24.3(5) |
| O13–C2–N3–C8 | 179.9(5) | 172.8(4) |
| O13–C2–N3–C9 | −1.7(8) | 1.5(7) |
| O14–C5–N6–C7 | −178.2(4) | 172.0(4) |
| O14–C5–N6–C18 | −3.3(7) | |
| C15–N1–C2–N3 | 172.2(4) | 176.8(3) |
| C15–N1–C2–O13 | −10.2(8) | −3.5(6) |
| C15–N1–C7–N6 | −57.2(5) | −57.2(4) |
| C15–N1–C7–C8 | −165.4(4) | −166.1(3) |
| C15–N1–C7–C12 | 71.4(5) | 70.2(4) |
| C15–C17–C18–O19 | | −12.9(6) |
| C15–C17–C18–C20 | | 167.9(3) |
| O16–C15–C17–C18 | | 116.0(4) |
| C17–C18–C20–C21 | | 175.7(4) |
| C17–C18–C20–C25 | | −3.8(6) |
| C18–N6–C7–N1 | 87.1(5) | |
| C18–N6–C7–C8 | −165.9(4) | |
| C18–N6–C7–C12 | −39.2(6) | |
| C18–C20–C21–C22 | 176.5(5) | −179.7(4) |
| C18–C20–C25–C24 | −177.0(5) | 180.0(4) |
| O19–C18–C20–C21 | −149.7(5) | −3.6(6) |
| O19–C18–C20–C25 | 26.6(7) | 177.0(4) |
| C20–C21–C22–C23 | 0.4(9) | −0.2(7) |
| C21–C20–C25–C24 | −0.6(8) | 0.5(7) |
| C21–C22–C23–C24 | −0.8(11) | 0.2(8) |
| C22–C23–C24–C25 | 0.6(12) | 0.1(9) |
| C23–C24–C25–C20 | 0.1(10) | −0.5(8) |
| C25–C20–C21–C22 | 0.4(8) | −0.2(6) |

idealized geometries, since they were not located in the refinement). This closed-shell close contact is relaxed to an estimated 2.89 Å in the crystallographic geometry (where ∠C5–N6–C18–C20 = +48°). It is also noteworthy that the phenyl ring twists relative to the plane of the attached carbonyl group by almost 30°, such that it becomes close to perpendicular to the plane through the attached 5-membered ring.

We have suggested that unfavorable interaction between the two oxygen atoms O16 and O19 may also contribute to the twist in **4a**, and that the ensuing induced asymmetry causes the bridgehead twist $\eta$ [10]. The current results support this hypothesis: the series of distances and angles at the acyl groups and around the N1–C7–N6 bridgehead exhibit the same qualitative trends as were described for **4a**. Thus, the N–C(=O) bond is longer in the twisted benzoyl group than in the planar acetyl group, ($d_{N6-C18} > d_{N1-C15}$). Consequently, the lone pair on N6 is expected to be more localized than that on N1, and N6–C7 is shorter than N1–C7 due to an anomeric-like effect (see Scheme 1 on p. 253 of Ref. [10]). Methyl group C12 is

Table 7
Ring puckering parameters, C11–C8–C7–C12 torsion angles, and conformations

| Compound | $\eta$ (°) | $\Xi$ (°) | $\tau$ (°) | $Q$ (Å) | $\phi$ (°) | Conformation |
|---|---|---|---|---|---|---|
| **4b** X-ray | −18.3 | 116.5 | | | | Ring **A** is almost a pure envelope (324°) with its apex at C7 pointing down*. |
| Ring A | | | −7.3 | 0.172 | 317.3 | Ring **B** is a pure envelope (288°) with its apex at C8 pointing down |
| Ring B | | | 44.8 | 0.142 | 288.6 | |
| **4b** RHF/3-21G | −30.5 | 108.0 | | | | Both rings are almost pure twist (306°). In ring **A** C7 is below* and C8 |
| Ring A | | | −4.8 | 0.250 | 301.9 | above* the N1–C2–N3 plane. In ring **B** C8 is below and C8 is above the |
| Ring B | | | 44.8 | 0.222 | 306.3 | N6–C5–N4 plane |
| **5b** X-ray | −24.3 | 111.8 | | | | Both rings are twist (126°). Ring **A** has C7 below and C8 above the N1– |
| Ring A | | | −7.2 | 0.209 | 127.3 | C2–N3 plane. Ring **B** has C8 below and C7 above the N6–C5–N4 plane |
| Ring B | | | | 0.206 | 128.8 | |
| **5b** RHF/3-21G | −25.7 | 109.8 | | | | Ring **A** is almost a pure twist (126°) with C7 below and C8 above the N1– |
| Ring A | | | −5.3 | 0.228 | 121.4 | C2–N3 plane. Ring **B** is an envelope (144°) with apex at C7 pointing up, |
| Ring B | | | | 0.215 | 137.4 | with some envelope character (126°) |

*Up* and *above* refer to the direction pointing to the concave side of the bicyclic system while *down* and *below* refer to the convex side.

thus pushed towards N1, giving rise to the non-zero value of $\eta$.

### 3.2. Experimental molecular geometry of **5b**

The crystal geometry of product **5b** represents the first direct determination of the geometry of a glycoluril condensation product. The results show that **5b** crystallizes in the keto form, since the two side-chain carbonyl groups are not coplanar, although a significant enol content was observed in solution by NMR. A superimposition of **3** and **5b** is shown in Fig. 6b. The resemblance is striking, and most of the features of the glycoluril core can be rationalized through explanations presented previously [10]. The benzoylacetyl group does not twist significantly around the C–N bond relative to the C2–N1–C7 plane; therefore, the aroyl moiety does not sterically interfere with amide planarity, in accord with its location above and away from the plane of the tetrahydroimidazole ring.

### 3.3. Comparison of experimental and optimized molecular geometries and crystal packing effects

The statistics in Table 8 clearly show a consistent picture of close reproduction of experimental bond lengths and angles by theory for both molecules. The torsion angles appear, however, to be less faithfully reproduced, especially with respect to the maximum and minimum deviations. Large deviations of certain optimized torsion angles from the experimental counterparts appear to be due to crystal packing effects.

As shown in Fig. 7a, each molecule of **4b** has close contacts in the crystal to three other molecules of **4b** and to one solvent ($CHCl_3$) molecule. The shortest non-hydrogen-to-non-hydrogen distance is that between the chloroform carbon atom and O14. The distance $O14{-}C_{chloroform} = 3.09$ Å is shorter than the sum of the van der Waals radii of an oxygen and a carbon atom (3.22 Å). The next shortest interaction is between a hydrogen atom bonded to C11 of the methyl group of one molecule and O13′ of another molecule. The C11···O13′ distance is 3.36 Å, slightly larger than the sum of the van der Waals radii. This contact may be a contributing factor to the deviation in the bridgehead angle $\eta$ which exhibits one of the largest positive experimental-optimized discrepancies (+12.2°). This is also consistent with the large negative discrepancies for torsions C2–N3–C8–N4 (−12.8°), C2–N3–C8–C7 and C2–N3–C8–C11, all of which are torsions surrounding C8. The third close contact is between O19 and a hydrogen on C10″

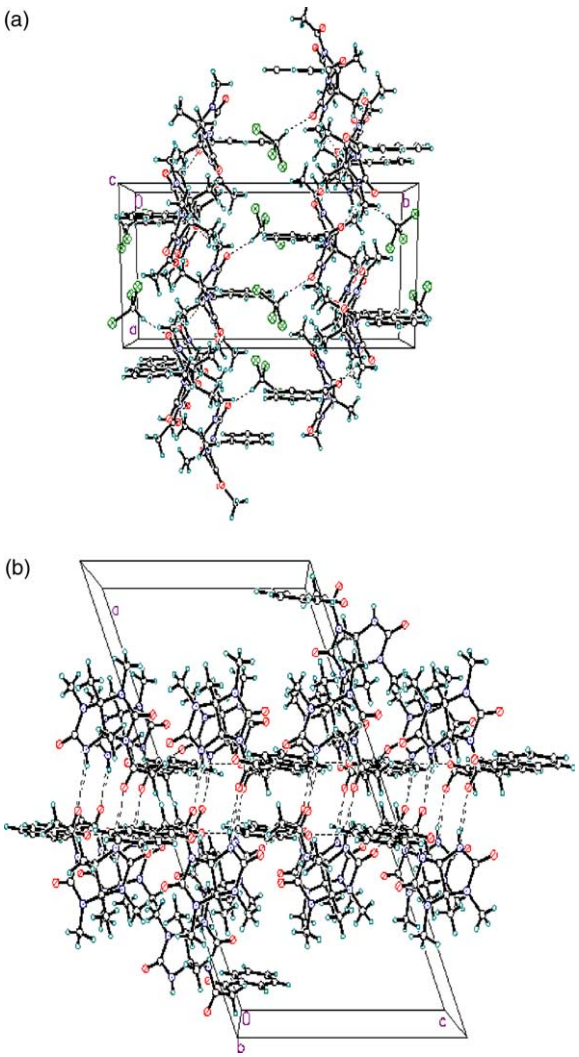


Fig. 2. Crystal packing diagrams for (a) **4b** and (b) **5b**.

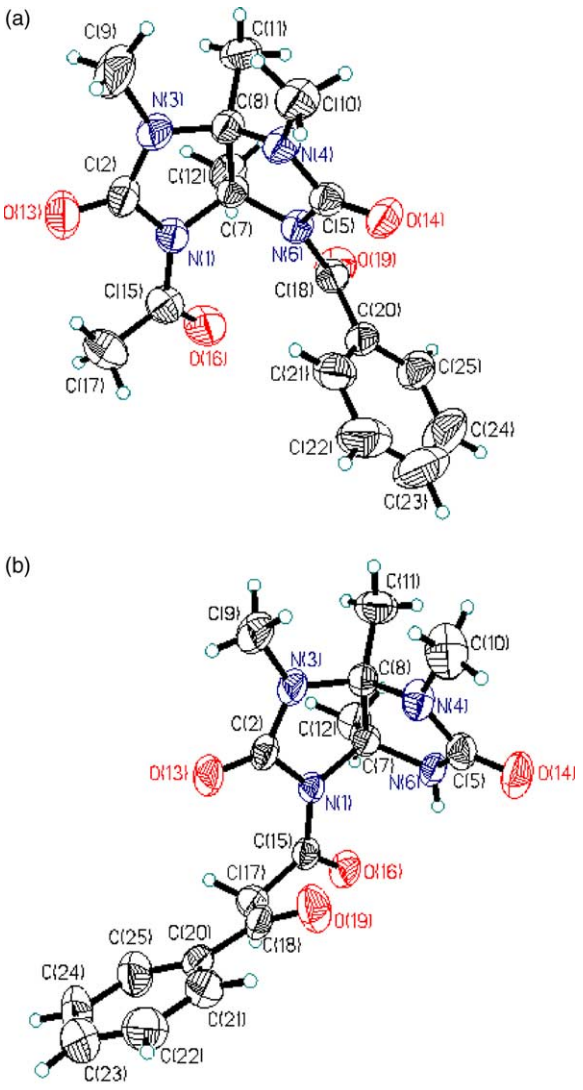


Fig. 3. Fifty percentage thermal ellipsoid diagrams for (a) **4b** and (b) **5b**.

of a third molecule with a O19–C10″ distance of 3.40 Å. Thus, packing appears to affect $\eta$ but not the amide twist angles $\tau$, an angle faithfully reproduced by calculation. Because both $\tau$ and packing affect $\eta$ independently, there is only a weak correlation between $\tau$ and $\eta$ in the diacylglycolurils that we have examined so far. Thus, although we had considered $\eta$ to be like the arm of a scale, measuring the relative 'weight' of electron density at N1 and N6, this correlation appears to be more complex than this original picture portrays. Clearly, the chloroform of crystallization in **4b** may also play a role in determining some of these torsion angles. Fig. 7b shows that **5b** forms dimers in the crystal, having two equivalent pairs of close contacts within each dimer. Thus, the molecules of **5b** are packed so that every molecule forms two close contacts to a single neighbor: N6–H···O16′ and N6′–H′···O16. The two close contacts are equivalent, with an N···O distance of 2.89 Å and an estimated angle N–

Table 8
Comparison statistics between experimental and optimized geometric parameters

| | | 4b | 5b |
|---|---|---|---|
| Bond length (Å) | $n$ | 27 | 27 |
| | Av.\|dev\| | 0.009 | 0.009 |
| | $\sigma$\|dev\| | 0.006 | 0.007 |
| | Av.dev | −0.003 | −0.006 |
| | $\sigma$dev | 0.010 | 0.010 |
| | Max.dev | 0.018 | 0.013 |
| | Min.dev | −0.024 | −0.024 |
| Bond angles (°) | $n$ | 44 | 43 |
| | Av.\|dev\| | 0.9 | 0.8 |
| | $\sigma$\|dev\| | 0.7 | 0.7 |
| | Av.dev | 0.0 | −0.1 |
| | $\sigma$dev | 1.1 | 1.1 |
| | Max.dev | 2.1 | 2.7 |
| | Min.dev | −3.0 | −2.5 |
| Torsion angles (°) | $n$ | 69 | 64 |
| | Av.\|dev\| | 5.4 | 4.3 |
| | $\sigma$\|dev\| | 4.2 | 5.8 |
| | Av.dev | −0.2 | −1.1 |
| | $\sigma$dev | 6.8 | 7.1 |
| | Max.dev | 12.2 | 20.7 |
| | Min.dev | −12.8 | −24.4 |

Dev refers to the deviation of the optimized parameter from its corresponding experimental value ($P_{i(\text{experimental})} - P_{i(\text{optimized})}$). Av.|dev| is the average absolute deviation defined as $\{\sum_{i=1}^{n} |P_{i(\text{experimental})} - P_{i(\text{optimized})}|\}/n$, where $P_i$ stands for the $i$th member of the set of $n$ geometrical parameters. $\sigma$ stands for standard deviation, it is given for the sets of absolute deviations as well as for the sets deviations. Max and Min refer to the largest and smallest deviations, respectively.

H···O = 158.2°, suggesting the possibility of hydrogen bonding. Such hydrogen bonding may be at the origin of the experimental-optimized discrepancy about the torsion angles C15–C17–C18–O19 (−13.3°), and C15–C17–C18–C20 (−14.0°). Also, in the same dimer, the phenyl ring is involved in two other equivalent pairs of close contacts between the *meta*- and *para*-hydrogen atoms of the phenyl ring of one molecule with O14 and O19 of the other member of the dimer, respectively. The only other significant discrepancies are all the torsion angles involving C10–N4, which include the largest positive and the largest negative deviations: C10–N4–C5–O14 (+20.7°) and C10–N4–C8–C11 (−24.4°), respectively. The origin of these large deviations around N4 is unclear, but may resemble that at N3 in **4b**. The small number of discrepancies implies that packing does not affect the gross structure dramatically in **5b**. This conclusion further supports the contention that the geometry of both **4b** and **5b** is the result primarily of intramolecular forces.

### 3.4. Atoms-in-molecules study of *4b*

The degree of electron delocalization from a region of space R into another R′ is described in terms of the extent to which the Fermi hole for the electrons in R is contained in R′ and vice versa, the Fermi hole being the physical manifestation of the Pauli principle [30,31, also recently reviewed in Ref. 32]. This measure of delocalization is given an atomic basis by defining non-overlapping bounded atomic regions within a molecule. A real-space partitioning of the molecular electron density into atoms separated by interatomic surfaces is a basic tenet of the quantum theory of AIM [33]. The interatomic surfaces satisfy the condition of zero-flux in the gradient vector field of the density, $\nabla\rho(\mathbf{r})\cdot\mathbf{n}(\mathbf{r}) = 0$, at every point $\mathbf{r}(x,y,z)$ and where $\mathbf{n}(\mathbf{r})$ is a normal vector to the surface [33]. Integration of the electron density over the volumes of such bounded atoms provides a non-arbitrary definition of atomic population from which atomic partial charges are obtained by subtracting the nuclear charge. One can also define an electron delocalization index $\delta(\Omega,\Omega')$ from the magnitude of the Fermi correlation between atom $\Omega$ and atom $\Omega'$, each bounded by zero-flux interatomic surfaces or by a chosen outer molecular isodensity envelope. The delocalization index is defined in terms of the product of the overlap integrals over both atomic regions [31]:

$$\delta(\Omega,\Omega') = \delta(\Omega',\Omega) = 4\sum_i \sum_j S_{ij}(\Omega)S_{ij}(\Omega'), \qquad (1)$$

where $\delta_{ij}(\Omega)$ is the overlap integral of a pair of spin orbitals over an atom $\Omega$. $\delta(\Omega,\Omega')$ equals the number of electron pairs shared between two atoms $\Omega$ and $\Omega'$, whether bonded (i.e. linked by a bond path, [35]) or not. For bonded atoms, δ can be identified as a 'bond order' when no substantial charge transfer occurs between the bonded atoms [34]. For example $\delta(\text{H},\text{H}) = 1.0$ in $H_2$ and $\delta(\text{N},\text{N}) = 3.0$

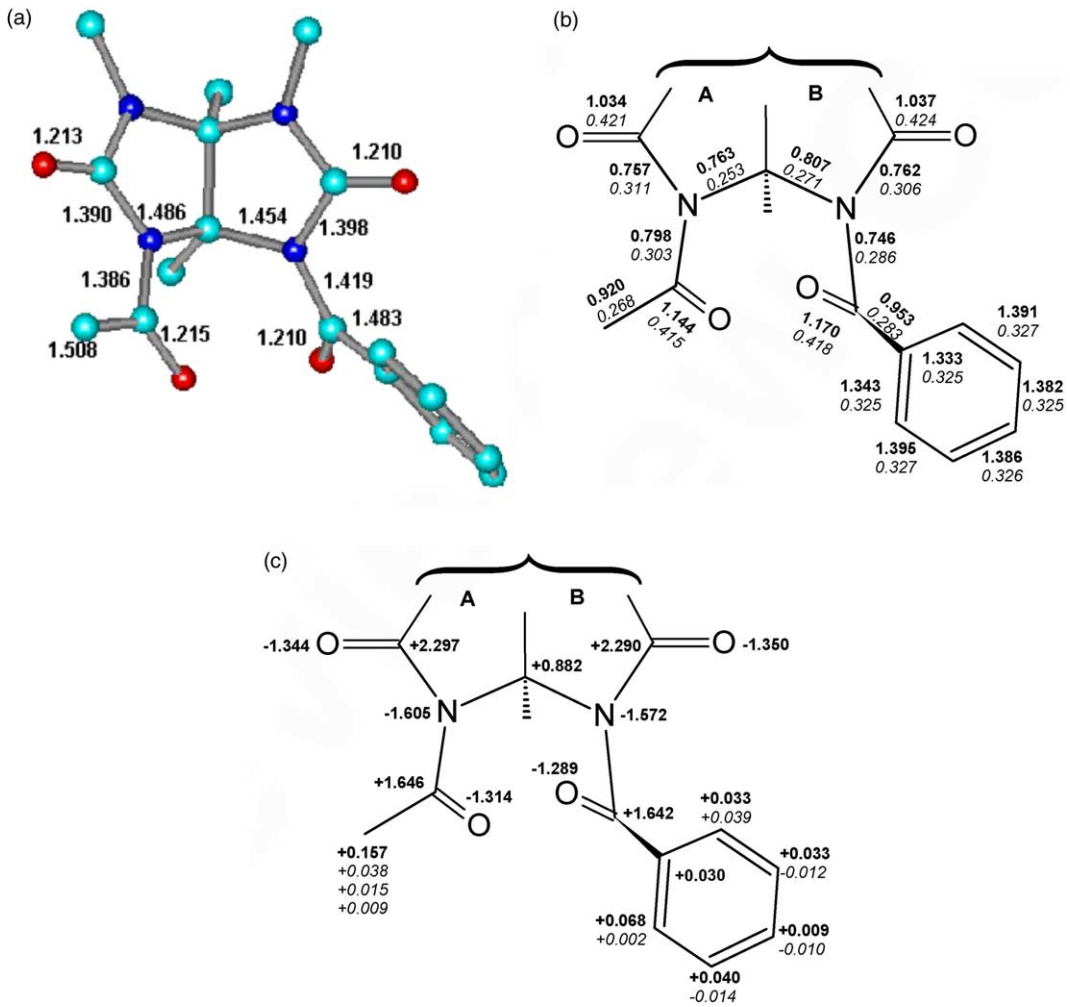


Fig. 4. (a) A view of the optimized geometry of **4b** with key bond lengths (Å) indicated. The distance O16–C18 = 3.248 Å; ∠O16–C18–O19 = 100.0°, equal to the Burgi–Dunitz angle; ∠C15–O16–C18 = 113.2°; and the dihedral angle between C18=O19 and the plane of the aromatic ring = 17.4°. (b) Delocalization indices ($\delta(\Omega,\Omega')$) between some bonded atoms (top, bold), and the electron density at the bond critical point $\rho_b$ in a.u. (bottom, italic). Values for bonds involving hydrogen atoms are omitted for clarity. (c) Some integrated atomic charges. When more than one figure is given, the top value (bold) refers to the carbon atom and the bottom value(s) (italic) to the hydrogen atom(s) bonded to it.

in $N_2$. Thus, $\delta = 1$ for an equally shared pair, but $<1$ when there is charge transfer as the pair becomes unequally shared due to charge disparity.

Trends in delocalization indices, a property of the pair density, generally parallel trends of the electron density at the bond critical point ($\rho_b$) [34]. It is important to distinguish between the information each of these two quantities conveys. $\rho_b$ is a measure of the accumulation of density between the two bonded atoms, pulling the nuclei toward each other. Thus, $\rho_b$ reflects the strength of the bonding and exhibits an inverse exponential relationship with the bond length [33].

The delocalization indices as well as the atomic charges in Fig. 4 are consistent with the previously proposed picture: the twisted amide has higher

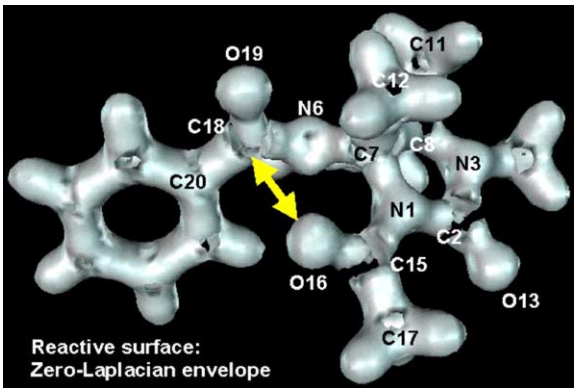


Fig. 5. Zero-Laplacian envelope of **4b**, showing the reactive surface. The O16–C18 interaction is shown (arrow).

$\delta$(C18, O19) than the acetyl group $\delta$(C15, O16), while the trend is reversed in the N–C(O) bonds. This reflects the greater delocalization of electrons from N to O in the planar amide than the non-planar structure. However, the ensuing higher negative charge on N6 than on N1 is not seen: the charges are calculated to be in the reverse order with N1 bearing a greater negative charge. Rather, the electronic effects of amide twisting are transferred directly to the anomeric carbon C7, as can be seen by the greater value of $\delta$(N6, C7) than $\delta$(N1, C7). This anomeric effect accounts for the large difference in the N1–C7 and N6–C7 bond lengths, as discussed previously (see Scheme 1 on p. 253 of Ref. [10]).

Another key feature of AIM is that all molecular properties are expressed in terms of corresponding densities, which can be integrated over atoms bounded by zero-flux surfaces to obtain additive atomic contributions to each molecular property [33]. One such property is the total molecular energy, which is partitioned into atomic energies ($E(\Omega)$), allowing one to track energetic changes in an area of interest within a molecule. A comparison of atomic energies of corresponding atoms of the amide groups on the two sides (**A** and **B**) of **4b** reveals that N1 is 39 kcal/mol more stable than N6, while O19 is more stable than O16 by 5 kcal/mol. The carbon atoms C15 and C18 have essentially identical energies (as expected from the similarity of their charges). The result is a net stabilization of the N–C=O group on

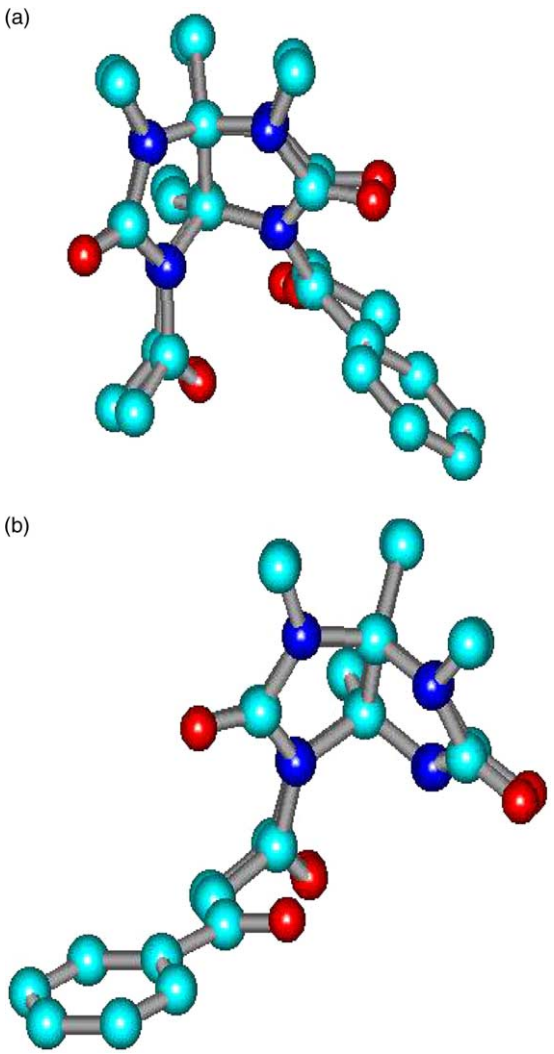


Fig. 6. Superimposition of experimental geometries for: (a) compounds **4a** and **4b** and (b) compounds **3** and **5b**.

the coplanar side **A**, over the twisted side **B** by 34 kcal/mol. In other words, the planar amide group which exhibits the higher degree of extended delocalization is more stable than its twisted counterpart.

From Fig. 4(b), it is clear that the individual delocalization indices between these carbonyl carbon atoms and their three bonded neighbors are different on sides **A** and **B**; however, their sum, $\delta$(C, O) + $\delta$(C, N) + $\delta$(C, C), is approximately equal for both sides (2.86 for C15 and 2.87 for C18). This indicates

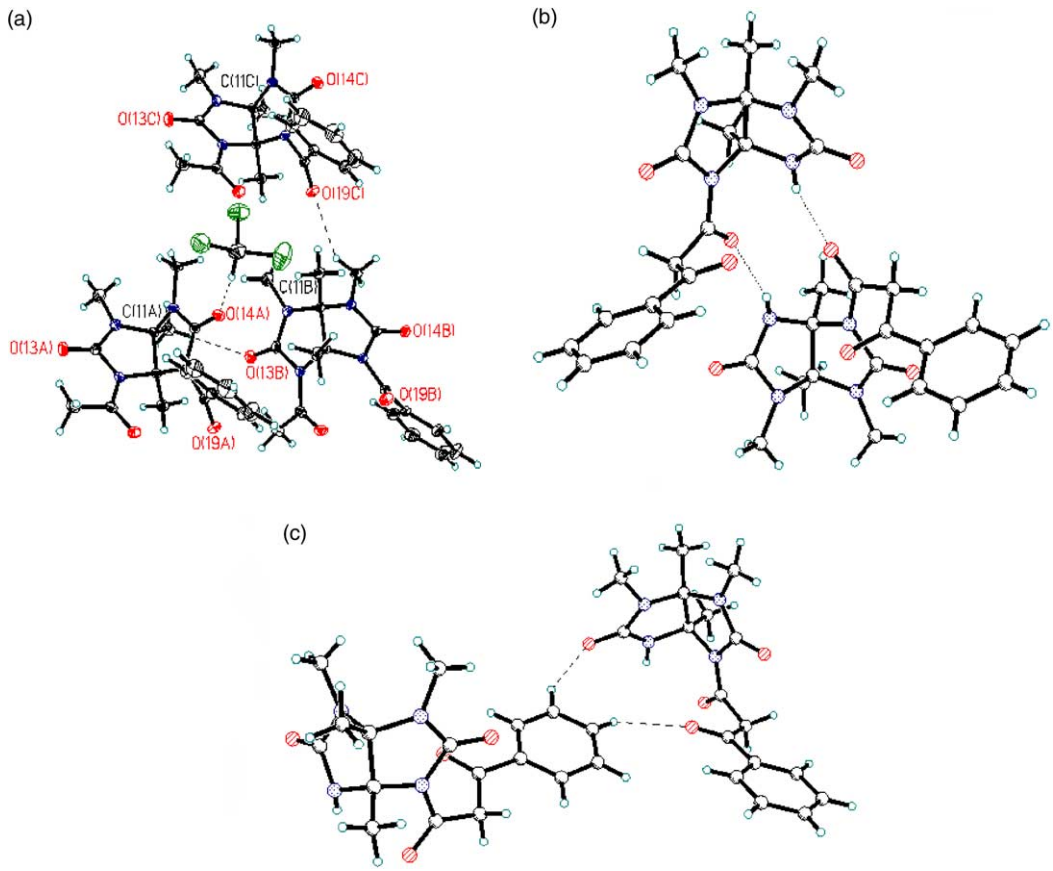


Fig. 7. (a) Crystal close contacts between molecules of **4b** and of $CHCl_3$; (b) Hydrogen-bonded dimers in **5b**; (c) various close contacts in **5b** (see text).

a reorganization of electron delocalization from the carbonyl carbon atom to its bonded neighbors, yet inducing a similar charge on each of the phenyl ring and the methyl (C17) groups (each carry a total charge of $+0.22e$).

Fig. 5 is a three-dimensional plot of the zero-Laplacian envelope of **4b**. The Laplacian of the electron density ($\nabla^2\rho(\mathbf{r})$), a three-dimensional second derivative of the electron density, magnifies subtle features in the density. It is convenient to define $L(\mathbf{r}) = -\nabla^2\rho(\mathbf{r})$, which is positive in nucleophilic regions of local charge concentration (local Lewis base) and negative in electrophilic regions of local charge depletion (local Lewis acid). The zero-Laplacian envelopes are nodes interfacing regions of density depletion and concentration. The last shell of charge concentration followed by charge depletion extending to infinity is called the valence shell charge concentration (VSCC), and is characterized by its nodal zero-Laplacian surface: the reactive surface (RS). When an atom is involved in bonding the spherical symmetry of the RS is broken and it may become punctured. A chemical reaction corresponds to the combination of a 'lump' in the RS of the base with the 'hole' in the RS of the acid [33].

In **4b**, the twisting of one amide relieves an unfavorable closed-shell close contact between two negatively charged oxygen atoms (O16 and O19); and also aligns one of the non-bonding VSCC (corresponding to the most probable position of a lone pair [36]) of the coplanar carbonyl oxygen (O16) with the electrophilic hole in C18 of the twisted carbonyl group (Figs. 5 and 8).

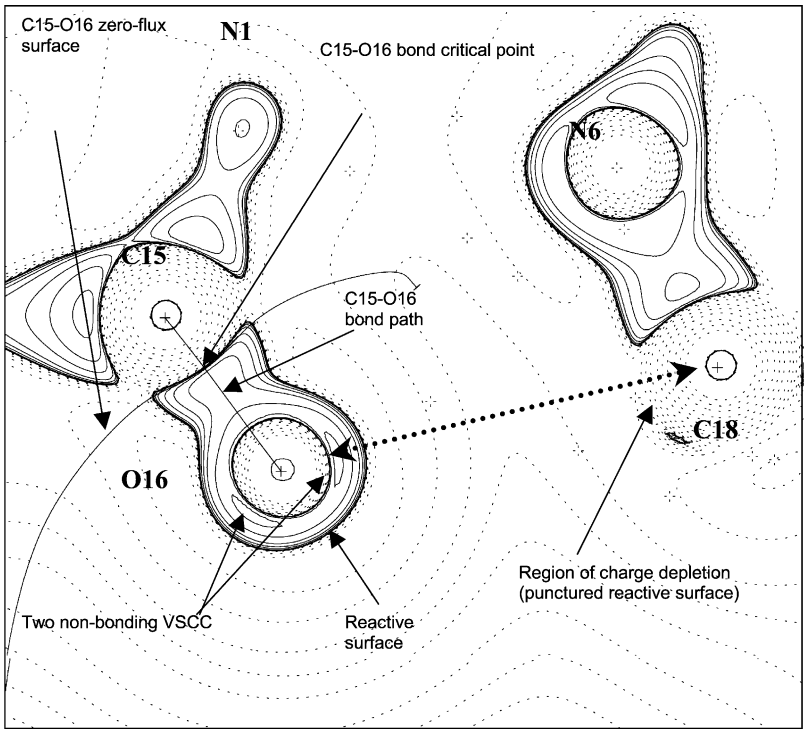


Fig. 8. Contour map of the negative of the Laplacian ($L(\mathbf{r}) = -\nabla^2\rho(\mathbf{r})$) for **4b** in the plane C15,O16,C18. All other atoms, being out of plane, have distorted contours. Positive and negative values of $L(\mathbf{r})$ are indicated by solid and dotted lines, respectively. One of the two non-bonded VSCCs of O16 (each corresponding to the most probable location of a lone pair) and the charge depletion in C18 fall on the same line connecting the nuclei. A line of maximum density linking the nuclei of any two bonded atoms (the bond path) is displayed between C15 and O16. Other bond paths are not displayed (out of plane). The curved line represents the intersection of the zero-flux surface separating O16 from C15 with the plane of the plot.

In effect, O16, C18 and O19 are positioned in an ideal geometry for transfer of the benzoyl group from N6 to O18 to generate an *O*-acyl enol ether. The lone pair at O16 points directly towards C18, and approaches the C18=O19 group at an angle of attack of 100°, close to the Burgi–Dunitz angle [37]. Only the large O16–C18 distance appears to prevent reaction. Thus, the two acyl groups in **4b**, held in proximity in order to promote reaction, interact in subtle ways. To summarize, the asymmetric disposition of the acyl groups with respect to the glycoluril core (with one coplanar and one out of plane) in diacylglycolurils alters the electronic balance between N1 and N6, driving the anomeric effect at C7 and the ensuing twist around the bridgehead, which nonetheless is also influenced by packing effects. The acyl groups come to the most stable geometry as a result of twisting being offset by reduced O···O non-bonded interaction, as well as a stabilizing O···C=O interaction.

### 3.5. Condensation reaction

The results show that as **4b** is converted to **5b**, amide torsional strain is relieved. The value of $\Xi$ decreases; as well, the ring geometries become more puckered (higher values of $Q$) and $\eta$ increases. The results thus support the hypothesis that the release of this torsional stain drives for the observed fast and irreversible condensation reaction. However, it is well known that the irreversibility of intermolecular Claisen and related condensations is driven by deprotonation at the acidic position between the carbonyl groups in the product [38]. Whether torsional strain relief provides significant thermodynamic drive for overall conversion in the present

case remains a question which can now be explored through further experimental study.

By contrast, selectivity and kinetic efficiency in this reaction are presumably determined largely when enolate **6b** undergoes intramolecular nucleophilic attack. The results show that although O16 is held in an ideal orientation for nucleophilic attack at C18 in **4b**, the large interatomic distance imposed by the glycoluril core precludes reaction. By extension, enolate **6b** must also have a large O to C distance which then explains lack of O-acylation. By contrast, C-acylation has a different geometric requirement: the $\pi$ orbitals of the enolate carbon atom C17 would lie above and below the C17–C15–O16 plane, in a region of space where they can readily overlap the vacant $\pi^*$ orbital of carbonyl group C18=O19. Thus the crystal structures suggest an explanation for the observed selectivity for formation of **5b**. This hypothesis can now be tested through a combination of kinetics and further crystal structures and AIM study.

## 4. Conclusion

The present study was undertaken as part of a broader goal of understanding the geometric requirements of acyl groups attached to the glycoluril system, as well as to probe the transition-state structure in intramolecular carbonyl condensation reactions. The crystal geometries suggest that torsion around the N–C(=O) bond may play a role in the promotion of the intramolecular condensation in these systems. Compound **4b** reported herein provides a base structure for comparison with other substituted acetyl aroyl glycolurils which have already been studied in kinetics experiments. The geometry of **4b** is notable for the increased acyl twist over **4a** as a result of substituting benzoyl for acetyl, while **5b** exhibits a lack of twisting consistent with an exothermic and irreversible conversion of **4b** to **5b**. The origin of the asymmetric acyl twist lies in a combination of avoiding close-shell contacts between the carbonyl oxygen atoms which carry similar charges, and generating a favorable interaction between one carbonyl oxygen and the other carbonyl carbon. The results suggest that asymmetry about the bridgehead-to-bridgehead bond, as measured by $\eta$, is a complex phenomenon caused by both acyl twisting and crystal packing effects. The electronic asymmetry introduced by substituents having different capacities to exchange electrons with the carbonyl groups leads to the twisting of the carbonyl group bonded to the substituent with the higher capacity to exchange electrons. Twisting of the benzoyl group in **4b** favors the alignment of non-bonding VSCC of the untwisted acetyl carbonyl oxygen atom O16 with the center of charge depletion on C18, an alignment that occurs at the Burgi–Dunitz angle.

## Acknowledgements

Financial support from the Natural Sciences and Engineering Research Council of Canada (NSERC) is gratefully acknowledged. Dr Jim Britten (McMaster) is thanked for diffraction data collection.

## References

[1] For recent reviews, see: J. Staunton, K.J. Weissman, Nat. Prod. Rep. 18 (2001) 380. B.J. Rawlings, Nat. Prod. Rep. 18 (2001) 190, and previous articles in this series.
[2] H. Biltz, Chem. Berichte 40 (1907) 4806.
[3] S. Sun, P. Harrison, Tetrahedron Lett. 33 (1992) 7715.
[4] C.N. Cow, P.H.M. Harrison, J. Org. Chem. 62 (1997) 8834.
[5] C. Cow, D. Valentini, P. Harrison, Can. J. Chem. 75 (1997) 884.
[6] S. Sun, P. Harrison, J. Chem. Soc., Chem. Commun. (1994) 2235.
[7] S. Sun, L. Edwards, P.H.M. Harrison, J. Chem. Soc., Perkin Trans. 1 (1998) 437.
[8] M. Rahimizadeh, K. Kam, S.I. Jenkins, R.S. McDonald, P.H.M. Harrison, Can. J. Chem. 80 (2002) 517.
[9] S. Sun, J.F. Britten, C.N. Cow, C.F. Matta, P.H.M. Harrison, Can. J. Chem. 76 (1998) 301.
[10] C.F. Matta, C.C. Cow, S. Sun, J.F. Britten, P.H.M. Harrison, J. Mol. Struct. 523 (2000) 241.
[11] C.N. Cow, J.F. Britten, P.H.M. Harrison, Chem. Commun. (1998) 1147.
[12] P.A. Duspara, C.F. Matta, S.I. Jenkins, P.H.M. Harrison, Org. Lett. 3 (2001) 495.
[13] S. Xu, P.K. Gantzel, B. Clarck, Acta Crystallogr. C50 (1994) 1988.
[14] N. Li, S. Maluendes, R.H. Blessing, M. Dupuis, G.R. Moss, G.T. DeTitta, J. Am. Chem. Soc. 116 (1994) 6494.
[15] V.L. Himes, C.R. Hubbard, A.D. Mighell, Acta Crystallogr. B34 (1978) 3102.

[16] N. Modrić, M. Poje, Acta Crystallogr. C51 (1995) 2594.
[17] M.O. Dekaprilevich, L.I. Suvorova, L.I. Khmelnitskii, Acta Crystallogr. C50 (1994) 2056.
[18] J. Boileau, E. Wimmer, R. Gilardi, M.M. Stinecipher, R. Gallo, M. Pierrot, Acta Crystallogr. C44 (1988) 696.
[19] A variety of molecular clips and cucurbituril derivatives exhibit this phenomenon. For reviews see: (a) R.P. Sijbesma, R.J.M. Nolte, Top. Curr. Chem. 175 (1995) 25. (b) W.L. Mock, Top. Curr. Chem. 175 (1995) 1.
[20] J.D. Dunitz, X-Ray Analysis and the Structure of Organic Molecules, Cornell University Press, Ithaca, 1979, pp. 328–337.
[21] S. Yamada, Angew. Chem. Int. Ed. Engl. 32 (1993) 1083.
[22] (a) For reviews, see:S. Yamada, in: A. Greenberg, C.M. Breneman, J.F.E. Liebman (Eds.), The Amide Linkage, Wiley, New York, 2000, pp. 215–246. (b) S. Yamada, Rev. Heteroatom Chem., 19, 1999, pp. 203.
[23] R.H. Lideman, P.F. Merenda, R.Z. Gold, Introduction to Bivariate and Multivariate Analysis, Scott Foresman, Glenview, IL, 1980, pp. 93–108.
[24] D. Cremer, J.A. Pople, J. Am. Chem. Soc. 97 (1975) 1354.
[25] D. Cremer, RING program, Quantum Chemistry Program Exchange No. QCMP 110, Indiana University, Bloomington, Ind., USA.
[26] M.J. Frisch, G.W. Trucks, H.B. Schlegel, P.M.W. Gill, B.G. Johnson, M.A. Robb, J.R. Cheeseman, T. Keith, G.A. Petersson, J.A. Montgomery, K. Raghavachari, M.A. Al-Laham, V.G. Zakrzewski, J.V. Ortiz, J.B. Foresman, C.Y. Peng, P.Y. Ayala, W. Chen, M.W. Wong, J.L. Andres, E.S. Replogle, R. Gomperts, R.L. Martin, D.J. Fox, J.S. Binkley, D.J. Defrees, J. Baker, J.P. Stewart, M. Head-Gordon, C. Gonzalez, J.A. Pople. GAUSSIAN94, Revision B.3, Gaussian Inc., Pittsburgh, PA, 1995.
[27] F.W. Biegler-König, R.F.W. Bader, T.-H. Tang, J. Comput. Chem. 13 (1982) 317 (http://www.chemistry.mcmaster.ca/aimpac/).
[28] C.F. Matta, *AIMDELOC01* (QCPE0802) Quantum Chemistry Program Exchange, Indiana University, Bloomington, 2001 (http://qcpe.chem.indiana.edu/).
[29] HyperChem, HyperCube, Inc., Canada, 1996.
[30] R.F.W. Bader, A. Streitwieser, A. Neuhaus, K.E. Laidig, P.J. Speers, Am. Chem. Soc. 118 (1996) 4959.
[31] X. Fadera, M.A. Austen, R.F.W. Bader, J. Phys. Chem. A 103 (1999) 304.
[32] C.F. Matta, J. Hernández-Trujillo, R.F.W. Bader, J. Phys. Chem. A 106 (2002) 7369.
[33] R.F.W. Bader, Atoms in Molecules: A Quantum Theory, Oxford University Press, Oxford, UK, 1990.
[34] C.F. Matta, J. Hernández-Trujillo, J. Phys. Chem. A (2003) in press.
[35] R.F.W. Bader, J. Phys. Chem. A 102 (1998) 7314.
[36] R.F.W. Bader, G.L. Heard, J. Chem. Phys. 111 (1999) 8789.
[37] H.B. Burgi, J.D. Dunitz, E.J. Shefter, Am. Chem. Soc. 95 (1973) 5065.
[38] (a) J. March, Advanced Organic Chemistry, fifth ed., Wiley, New York, p. 571. (b) J.F.J.GarstChem. Educ.561979721. (c) J.F.J.Garst, Chem. Educ. 56 (1979) 721.